




# Information Inversion and Dynamic Analysis of Video-Driven Fire Detection Based on Object-Oriented Segmentation

Yanying Cheng , Hui Bai, Zhisheng Li, Yuchun Zhang\*, Longfei Chen\* and Ke Chen, Faculty of Geoscience and Environmental Engineering, Southwest Jiaotong University, Chengdu 610031, China

**Received:** 1 July 2021/**Accepted:** 6 January 2022/**Published online:** 2 February 2022

**Abstract.** During an emergency response to a sudden fire, the video-driven techniques for detection and real-time analysis can significantly affect the scientificity and effectiveness of disposal, thus changing the process of fire rescue. In this paper, an information inversion model for video-driven fire based on object-oriented segmentation has been proposed and programmed with Python. Firstly, a video fire detection algorithm based on deep learning was adopted. Secondly, fire regions were segmented using the SEEDS superpixel-based method, from which the flame size with time was further extracted. Then the heat release rate was inverted over time. Finally, the fire development was analyzed based on the characteristics of flame images. The model was applied to three different types of fire, a diesel pool fire, a propane fire, and a full-scale wood crib fire. The results indicated that the model could achieve real-time information such as flame height, projection area, and volume, and the spatial-temporal evolution laws could be further estimated quickly. Committed to intelligent analysis of fire environment based on surveillance cameras, the model can provide technical assistance for fire-fighting and on-site emergency rescue.

**Keywords:** Superpixel segmentation, Emergency response, Video-driven fire, Fire development, Information inversion

## 1. Introduction

In recent years, with the rapid development of computer vision technology, video-based fire detection (VFD) technology has attracted extensive attention of scholars. The technology mainly consists of four steps: video image acquisition, image preprocessing, fire detection algorithm, and fire signal output, as shown in Fig. 1. Compared with the traditional fire detection methods such as heat detector, smoke detector, and optical flame fire detector, VFD has the advantages of wide monitoring range, quick response speed, accurate detection, rich and intuitive information, etc. [1, 2].

---

\*Correspondence should be addressed to: Yuchun Zhang, E-mail: [zycfire@swjtu.edu.cn](mailto:zycfire@swjtu.edu.cn); Longfei Chen, E-mail: [longfeichen@swjtu.edu.cn](mailto:longfeichen@swjtu.edu.cn)





**Figure 1. Program flow of VFD.**

The VFD technology originated from image-type fire detectors using image processing technology for fire images' color or texture features. Huang et al. [3] adopted color and motion information extracted from video sequences to detect fire. Chen et al. [4] proposed an early fire detection method using an RGB model-based chromatic and disorder measurement for extracting fire-pixels and smoke-pixels. Qureshi et al. [5] presented QuickBlaze, a real-time early fire detection system, using parallel image processing streams to detect flame and smoke regions at high speed.

With the development of machine learning such as support vector machine (SVM), naive Bayes, random forest, and artificial neural network (ANN), the VFD has entered a new stage. Yang et al. [6] used an SVM approach for vessel fire detection, which used chromatics, area, perimeter, and rotundity rate of fire regions for model training. Wang et al. [7] developed a flame detection approach based on robust features and randomness testing, using seven features integrated by color and motion probabilities of flame candidates.

Due to the development of convolutional neural networks (CNN), many scholars have begun to use deep learning for fire detection. Wu et al. [8] presented an intelligent fire detection approach through cameras for preventing fire hazards from going out of control in chemical factories and other high-fire-risk industries, which adopted two CNNs to achieve a high detection rate and a low false alarm rate. Zhang et al. [9] proposed a lightweight model for forest fire detection based on attention U-Net and SqueezeNet. Li and Zhao [10] made a detailed comparison of object detection CNN models of Faster-RCNN, R-FCN, SSD, and YOLO v3 for fire detection and got some meaningful conclusions. Lin et al. [11] developed a joint detection framework based on Faster-RCNN and 3D CNN.

There have been some relevant studies and recently published reports on fire video analysis. Verstockt et al. [12] obtained smoke layer height using discrete wavelet transform (DWT)-based function and got the flame width and height based on the Otsu segmentation method. Thus, the heat release rate (HRR) can be estimated through the empirical formula summarized by Heskestad [13]. Their method was successfully used in an ISO 9705 room-corner test of a single-seat sofa. By assuming flames as trapezoids within the rack storage and as a truncated cone above the top fuel surface, Xin [14] developed an HRR estimating methodology in rack storage fire using flame volume. The results demonstrated that the flame-volume-based method could capture fire growth and suppression trends qualitatively, but it has not been automated. Using the image recognition technique on flame videos, Li et al. [15] proposed a computational model to estimate fire information for pool fires. The flame pulsation frequency was calculated first by fast Fourier transform (FFT) algorithm, and then, pool diameter, mean flame height, HRR, and fuel type were inversed with traditional fire dynamics theories.

Tarek Beji [16] estimated the HRR of a cable tray fire through the temporal evolution of flame and extinction front at the level of each tray, using video fire analysis technique.

Above all, scholars have made remarkable achievements in the accuracy and computational efficiency of VFD. However, most of the current research can only judge whether a fire occurs or not, while research on information inversion of video-driven fire, such as fire size, HRR, and development trend, is still insufficient and cannot be fully applied to the actual fire scenes. Nowadays, with the development of real-time monitoring technology and popularization of surveillance cameras, it is expected to mine rich and valuable information timely from fire videos, in order to provide strong support for fire-fighting and emergency response.

In this work, an intelligent inversion model of video-driven fire was proposed and successfully applied in three typical fire tests. The main contributions include: By adopting the SEEDS superpixel-based method, flame regions were efficiently segmented from images identified through a VFD model. Then, the HRR was inversely estimated from the flame size of height, area and volume derived from video images. On this basis, the spatial-temporal evolutions of the wood crib fire were further analyzed. The results indicate that the proposed model can provide automatic analysis of fire parameters based on video and contribute to an in-depth understanding of fire circumstances in emergencies.

## **2. Information Inversion Model Based on Object-Oriented Segmentation**

In the paper, a depth information inversion model for video fire based on object-oriented segmentation is constructed, which includes three parts: video-based fire detection, flame segmentation based on superpixel, and acquisition of fire characteristic dimension. The proposed model is realized through programming with Python 3.

### **2.1. Video-Based Fire Detection**

Firstly, a multi-scale deep learning network [17] based on LeNet is introduced for fire detection on the input video frames. Compared with other excellent and complex networks, LeNet has fewer parameters and is more efficient in training and testing. The detailed structure of CNN is shown in Fig. 2. Due to the added layer with spatial pyramid pooling, the network reduces the semantic difference of multi-scale space and achieves multi-scale expression of flame features. After iterative training on a particular data set of 10,000 images, the network performs a recognition accuracy of 93.30% for a test set of 1000 images, while the LeNet without a layer of spatial pyramid pooling reaches only 77.3% under the same training conditions.

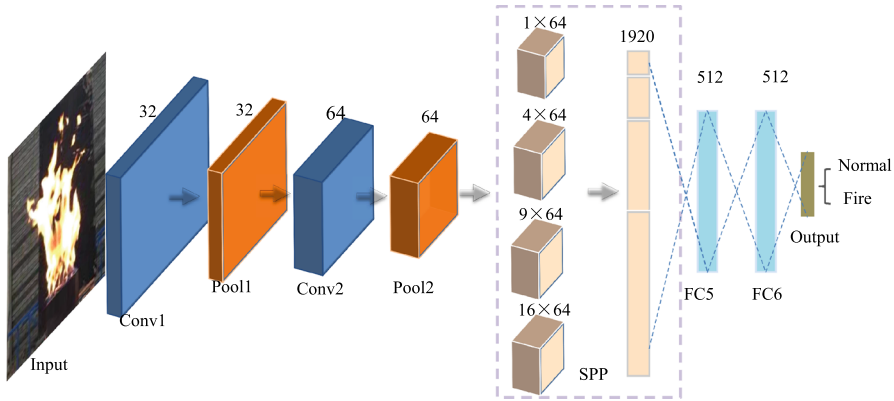


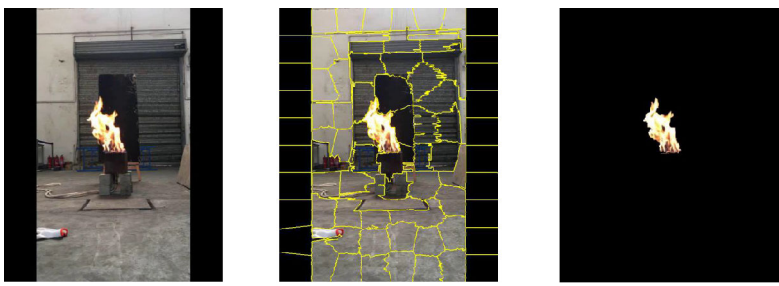
**Figure 2. Architecture of multi-scale CNN.**

**2.2. Flame Segmentation Based on Superpixel**

The process of flame segmentation mainly includes two parts: superpixel segmentation and color analysis. The steps are depicted in Fig. 3, and the detailed process is as follows.

**2.2.1. Superpixel Segmentation** By combining adjacent pixels with similar texture, color, brightness, and other characteristics, superpixel segmentation algorithms aim to build irregular pixel blocks with particular visual significance. We can directly operate on the divided superpixel regions instead of just pixels, thus reducing computational cost and algorithm complexity and improving computing efficiency. Researchers have conducted a lot of research and put forward several superpixel algorithms [18–22] such as Turbopixel, SLIC, LSC, GLSC, SEEDS, MeanShift, and Ncut.

As one of the best algorithms for superpixel segmentation, the SEEDS algorithm focuses on color information, which is the most prominent visual feature of fire images. Therefore, this paper adopts the SEEDS algorithm for flame segmen-



(a) original image      (b) superpixel segmentation      (c) flame segmentation

**Figure 3. Image segmentation based on superpixel and YCbCr color space.**

tation. The method initially sets a regular superpixel partition, and the optimization process is then performed based on a hill-climbing algorithm by moving the superpixel boundary. The objective function to measure each superpixel is given by

$$E(s) = H(s) + \gamma G(s) \quad (1)$$

where  $H(s)$  denotes the color distribution of each superpixel module with histogram statistics, and its value increases with the concentration and singleness of color distribution.  $G(s)$  is a shape expression that represents the regularity degree of superpixel. And  $\gamma$  is a coefficient, employed to adjust the weight of color and shape.

**2.2.2. Color Analysis** A prior criterion based on flame color is adopted to segment the superpixel-level image further. Specifically, the color-based judgment criterion presented by Celik and Demirel [23] is employed in the YCbCr color space.

$$\left\{ \begin{array}{l} Y(x, y) > Y_m(x, y) \\ Cr(x, y) > Cr_m(x, y) \\ Cb(x, y) > Cb_m(x, y) \\ Y(x, y) > Cb(x, y) \\ Cr(x, y) > Cb(x, y) \\ |Cr(x, y) - Cb(x, y)| \geq \tau \end{array} \right. \quad (2)$$

where  $Y(x, y)$ ,  $Cr(x, y)$ ,  $Cb(x, y)$  are brightness, redness, and blueness of the pixel  $(x, y)$ , respectively, to which  $Y_m$ ,  $Cr_m$ ,  $Cb_m$ , respectively, correspond to mean value. And  $\tau$  represents the threshold, which is 40 in this article. Compared with others, the YCbCr color model is less affected by light and similar to the cognitive pattern of the human visual system.

### 2.3. Acquisition of Fire Characteristic Dimension

In order to get useful real-time fire information, the key is to derive time-varying size characteristics from segmented flame images [24–29], such as flame height, area, centroid coordinates, circularity, and rectangularity. The three features used in this article are listed below in detail.

**2.3.1. Flame Height  $L_{flame}$**  Flame height is the visible length of flame in the vertical direction, which is the most intuitive and helpful information for fire images.  $L_{flame}$  is the actual physical height as a function of time, converted from the vertical length of flame in the image coordinate system.

$$L_{flame} = \alpha \cdot L_{pixel} \quad (3)$$

where  $L_{pixel}$  is the pixel length of flame.  $\alpha$  is the scale of pixel distance and space distance, which can be obtained by camera calibration.

**2.3.2. Projected Area of Flame  $S_{flame}$**  The projected area refers to the size of image space occupied by flame projected from three-dimensional space to the two-dimensional plane of a camera. The actual  $S_{flame}$  is given by multiplying the sum of pixels in the segmented flame region  $f(x,y)$  by the square of the corresponding scale.

$$S_{flame} = \alpha^2 \cdot \sum_{x=0}^{n-1} \sum_{y=0}^{m-1} f(x,y) \quad (4)$$

where  $m, n$  are the height and width of the digital image, respectively.

**2.3.3. Flame Volume  $V_{flame}$**   $V_{flame}$  is the volume of flame in three dimensions. Based on the idea of multi-layer cylinder superposition, the geometry of an axisymmetric flame is assumed to be a polyhedron composed of  $L_{pixel}$  discrete small cylinders [24, 25]. The  $V_{flame}$  is calculated by

$$V_{flame} = \alpha^3 \cdot \sum_{i=1}^{L_{pixel}} \frac{\pi}{4} D(i)_{flame}^2 \quad (5)$$

$$D(i)_{flame} = \left[ \sum_{j=1}^m (x_{2j} - x_{2j-1})^2 \right]^{1/2} \quad (6)$$

where  $D(i)_{flame}$  is the pixel equivalent diameter of the  $i$ th cylinder,  $m$  is the total number of flamelet disks, and  $x_{2j}$  and  $x_{2j-1}$  are the adjacent abscissae of a flamelet disk.

### 3. Results and Discussion

Three typical fuels, i.e., wood crib, diesel, and propane (Fig. 4), were selected as representatives of different types of solid, liquid, and gas fire, and combustion videos were taken, respectively. Through the method described in Chapter 2, the identified flame areas were segmented by superpixel method, and useful information was further automatically extracted in three videos.

#### 3.1. Experimental Design

The working conditions of the three different fire experiments are given in Table 1. The entire process is monitored by a CCD camera with a frequency of 30 frames per second. In Test 1, there is an electronic balance under the oil pool to record the real-time quality of fuel. The fuel flow rate of Test 2 is set to a constant value to ensure stability during the combustion process. For Test 3, the standard wood crib (Fig. 5) is stacked by a total of 280 pieces of wood, with the dimension of 2.0 m × 2.0 m × 0.7 m (length × width × height). It is ignited at

the center of the bottom with a towel dipped in diesel oil. And a fire hose is turned on the wood crib at 1210 s when the fire begins to decay until extinguished. All three experiments are carried out in large indoor venues and can be regarded as fuel-controlled combustion.

3.2. Methods and Parameters of Object-Oriented Segmentation

There are many superpixel segmentation algorithms, among which SEEDS, SLIC, and LSC are the most prominent, but the application scenarios are different due to different principles. The XimgProc module of OpenCV version 3.4.1 is introduced to investigate the segmentation effect of SEEDS, SLIC, and LSC algorithms in different fire images, and all the experiments are carried out on a desktop computer with an Intel(R) Core (TM) i5-8400 @2.81 GHz processor and 8 GB of memory. The number of superpixels per image is set to be about 300, and the iteration number is set to 20. In this paper, qualitative and quantitative methods are used to check the performance of different superpixel algorithms in flame segmentation.

The visual comparison of three superpixel methods is illustrated in Fig. 6. Among the three methods, the SEEDS yields smoother flame boundaries on five sample images. The SLIC and LSC algorithms can also achieve good segmentation results and generate mostly regular superpixel blocks. However, they are con-

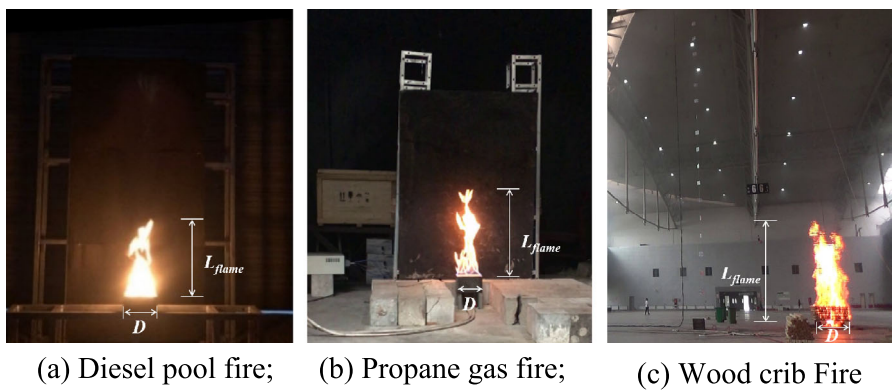
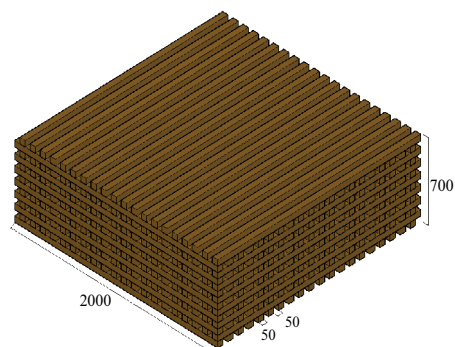


Figure 4. Typical experimental pictures.

Table 1  
List of Experimental Conditions

Test No	Fuel	Fire size/mm	Mass/g	Mass flow-rate/m <sup>3</sup> /h
1	Diesel	24.5 × 24.5	170	—
2	Propane	0.1 × 0.1	—	2.4
3	Wood crib	2000 × 2000 × 700	—	—





**Figure 5. The schematic diagram of wood crib.**

cerned about so many texture details in the layered region of inner flame and outer flame, and a lot of contour illusion is added to the irregular part around a flame. For quantitative analysis, flame segmentation precision (FSP) and recall (FSR) are used to investigate the accuracy of algorithms, referring to the achievable segmentation accuracy (ASA) [21, 30].

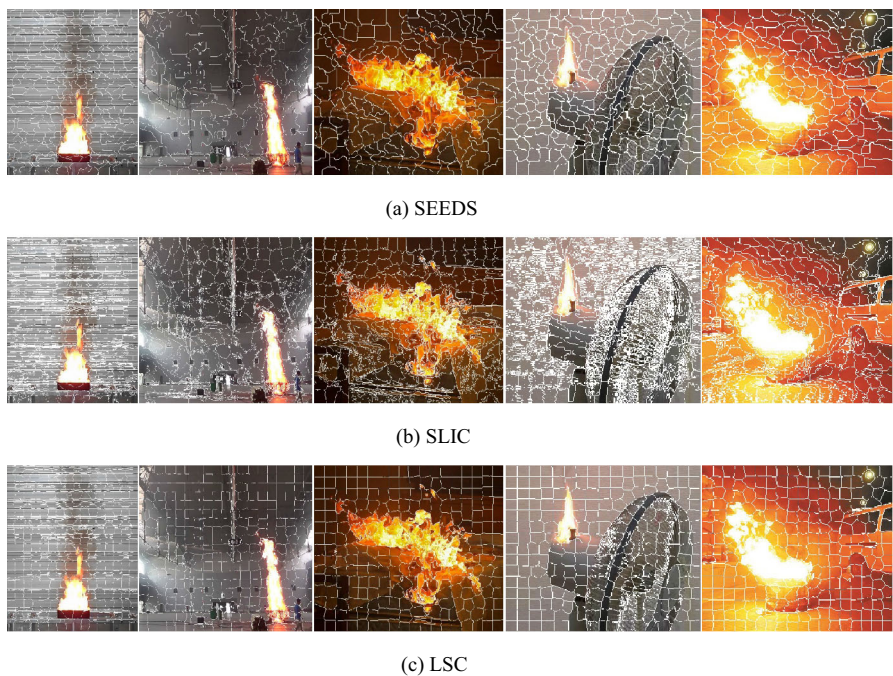


**Figure 6. Segmentation results of different superpixel algorithms.**



$$FSP = \frac{|S \cap G|}{|G|} \tag{7}$$

$$FSR = \frac{|S \cap G|}{|S|} \tag{8}$$

where  $S$  is the segmented flame region, and  $G$  is the grand truth segment.

Table 2 presents the average segmentation accuracy of three methods on the images shown in Fig. 6, as well as the average running time. The results show that the SEEDS method has high accuracy and recall rate with the highest time efficiency. Therefore, this paper chooses the SEEDS algorithm that has the best effect on fire scene segmentation.

Figure 7 illustrates the visual effect of superpixel segmentation under different settings. The description of edge segmentation varies significantly with different numbers, and it is disadvantageous for accurate and fast segmentation when the number of superpixels is too small or too much. The relation between the set value of superpixel and number of generations by SEEDS for this image is also discussed, as shown in Fig. 8. The results reveal the curve presents a step-like change, while the number of generated superpixels does not change as the set value increases within a specific range. In order to effectively preserve the boundary of the flame region and reduce the subsequent computation, it is suggested to select the setting value of superpixel in the intermediate state (e.g., Fig. 7c or d) in this paper.

3.3. Characteristic Parameter Analysis of Fire Images

Figures 9, 10, and 11 show the fire information of flame height, projected area, and volume, directly calculated by our method using Python program in three experiments. The size of fuel burners (Test 1 and Test 2) and the wood crib (Test 3) are, respectively, selected as the reference to get the scale between the video images and the actual scene. In addition, other markers of known size in the image, such as brackets, blocks, and trusses, are also used to verify the flame size. Due to the periodic pulsation characteristics of flame, the fire image information with an intermittent rate of 0.5 per second is also achieved and given on the height, area, and volume graphs. It should be noted that in actual fires, fire ima-

**Table 2**  
**Performance Metrics of Three Algorithms**

	<i>FSP</i>	<i>FSR</i>	Time/s
SEEDS	0.92	<b>0.95</b>	<b>0.11</b>
SLIC	0.91	0.93	0.15
LSC	<b>0.93</b>	0.94	0.84

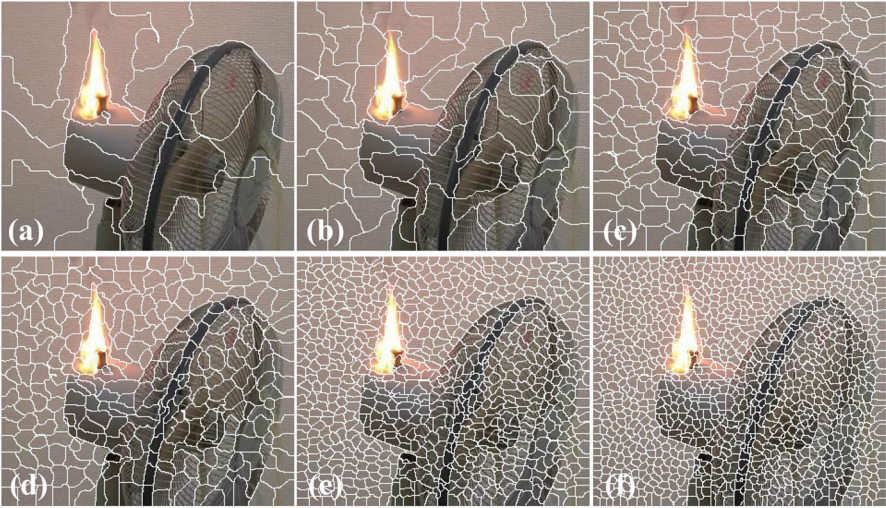


**Figure 7. Comparison of different numbers of superpixels: a  $N = 16$ ; b  $N = 72$ ; c  $N = 208$ ; d  $N = 304$ ; e  $N = 800$ ; and f  $N = 1287$ .**

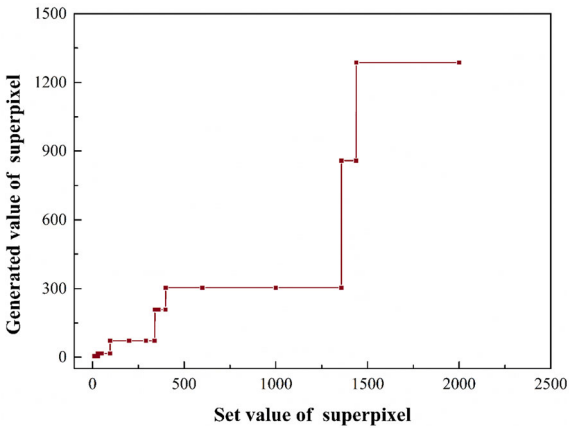


**Figure 8. Variation of generated superpixel number with the set value.**

ges or video clips can be extracted at intervals based on computing power and data complexity, instead of selecting each frame.

The curves of flame height, projected area, and volume over time are generally consistent in each fire test, showing an obvious rising, stable, and decline period in Tests 1 and 3. During Test 2, the curves present almost a straight line, respectively, which is caused by a constant flow rate of propane. Figure 9d illustrates the variation of diesel mass and mass loss rate over time, which directly reflects

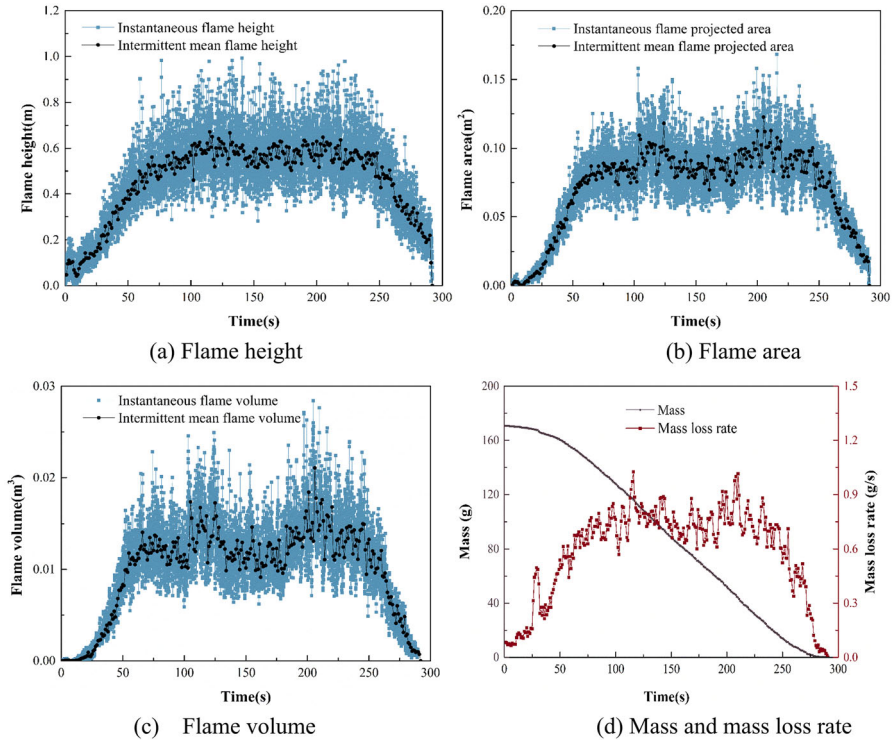


**Figure 9. Variation of diesel flame size with time.**

the change of HRR during the combustion. Due to fire-fighting intervention, the fire is extinguished rapidly in Test 3, resulting in a short decline period in Fig. 11.

### 3.4. HRR Inversion

The fire size is directly characterized by the real-time HRR. However, due to the complexity of fire scene, this value is generally challenging to get. In this paper, the real-time HRR is estimated inversely through the flame size, and the result is compared with the commonly used model. Pool fire is one of the hot topics in fire research, and many valuable conclusions have been drawn. The flame height model presented by Heskestad [13] (Eq. (9)) can be transformed into Eq. (10) to predict the fire power. In addition, the mass of diesel fuel is measured in Test 1, and HRR can be calculated through fuel flow rate, as indicated by Eq. (11).

$$\frac{L_{flame}}{D} = -1.02 + 0.23 \frac{Q_c^{2/5}}{D} \quad (9)$$

$$Q_c = (4.348L_{flame} + 4.435D)^{5/2} \quad (10)$$

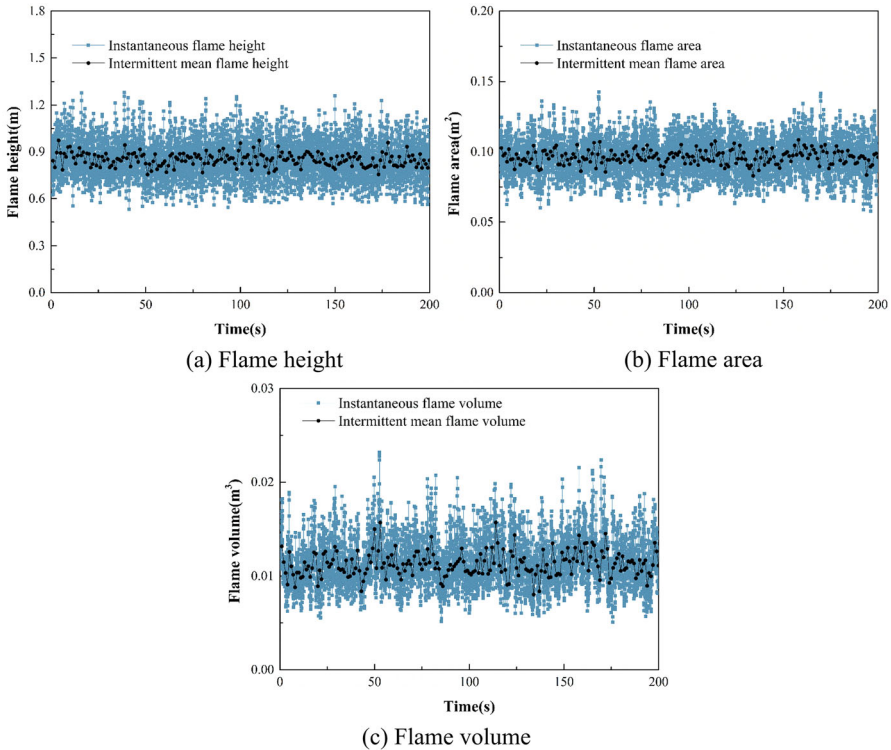


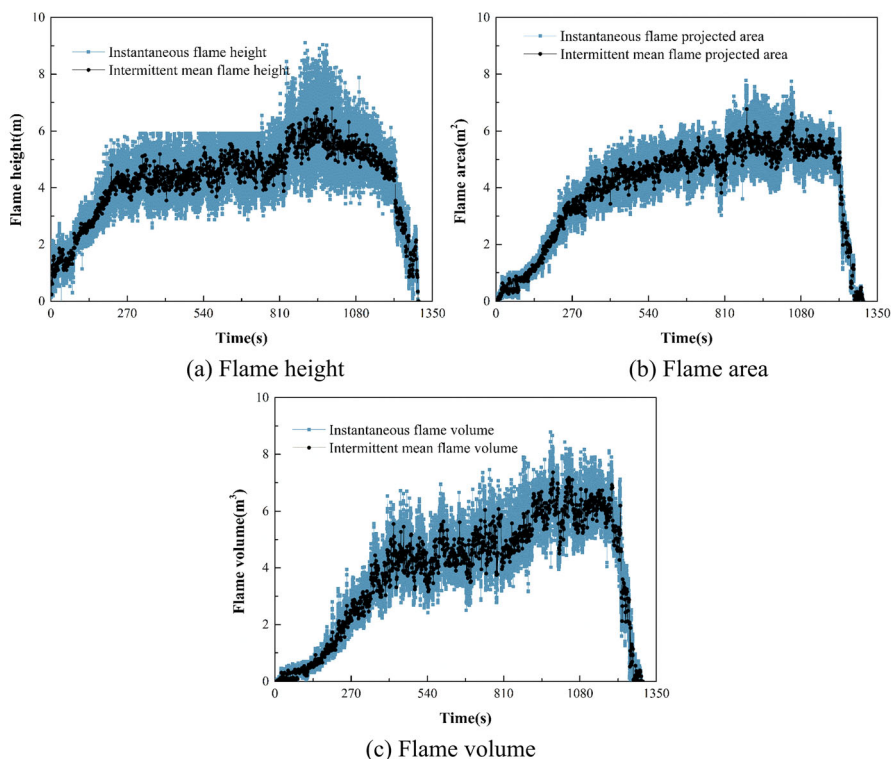
**Figure 10. Variation of propane flame size with time.**

$$Q_c = \dot{m} * \eta * H_c \quad (11)$$

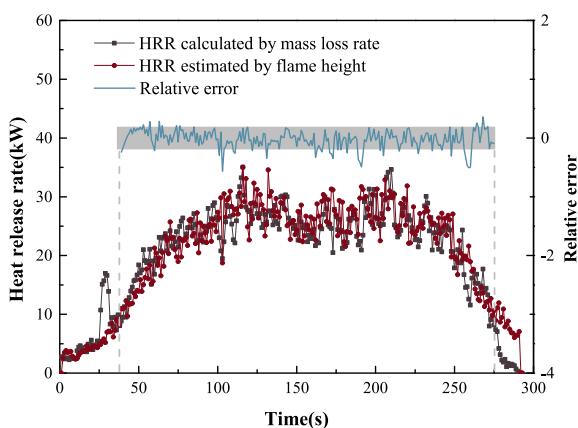
where  $Q_c$  is the HRR,  $D$  is the source diameter,  $\dot{m}$  is the mass loss rate of fuel burned, expressed in kg/s,  $\Delta H_c$  is the complete heat of combustion, and  $\eta$  is the combustion efficiency, which is set to 0.8 according to reference [25, 26].

Figure 12 shows the HRR with time obtained from the calculated approach of mass loss rate (Eq. (11)) and flame height (Eq. (10)). Since the two curves show good agreement in the figure, the relative error curve in the middle stage of the combustion process is also drawn for further analysis. As the figure shows, most of the relative errors are within  $\pm 20\%$  (the shaded part in the figure). We can conclude that the HRR of pool fire can be estimated directly from flame height as a surrogate, and the source diameter can be used as a reference for image distance and space distance. Nevertheless, there are still several points with large errors in the initial and extinguishing stages of fire, which may be caused by the significant change in the intermittent flame height due to the fluctuation of flicker frequency.

When the flow rate is fixed in terms of propane fire, the HRR maintains a constant value according to Eq. (12). The combustion efficiency in Test 2 is set as 100% due to the nearly complete combustion [31]. From Fig. 10, the flame size



**Figure 11. Variation of wood crib flame size with time.**



**Figure 12. Variation of HRR with time.**

remains unchanged within limits. The literature review [14, 25, 27, 32, 33] shows that there is a proportional relationship between HRR and flame volume under certain conditions, i.e.,

$$Q_c = q''' * V_{flame} \tag{12}$$

where the coefficient  $q'''$  is a constant, given in  $\text{kW/m}^3$ . Moreover, the value is calculated by simultaneous Eqs. (8) and (9), where  $4700 \text{ kW/m}^3$  is taken in Test 2. As a consequence, the actual HRR of propane with time can be estimated from the real-time flame volume, as shown in Fig. 13. Almost all HRR points estimated by flame volume fall within  $\pm 10\%$  range of the measured value (the shaded part in the figure) by mass flow, indicating the accuracy of the inversion model. For the value of constant  $q'''$ , scholars have given different suggestions [14, 25, 33]. According to our experience, this value varies greatly, especially for small fires, due to camera shooting conditions, flame segmentation algorithm, and volume calculation methods. Besides, the equivalent diameter method expressed in Eq. (6) makes the value of flame volume smaller than the direct external volume, which may not occur in a large-scale fire. Therefore, the coefficients  $q'''$  should be corrected appropriately for different scenes and image processing methods.

Similarly, the HRR of wood crib fire has also been measured using flame volume through Eq. (12). For the traditional HRR estimation based on oxygen consumption, the cone calorimeter, gas analyzer, thermocouples, and other devices should be reasonably arranged, which is always unavailable for large-scale fire experiments. Experiments on wood crib fire are hard to conduct repeatedly, and relevant empirical formulas are lacking but fail to apply in HRR estimation. Therefore, the constant  $q'''$  is set to be  $1100 \text{ kW/m}^3$  under similar conditions, which has been verified [14]. Thus, the HRR in the steady stage of the wood crib fire is estimated to be  $6 \sim 7 \text{ MW}$  in Test 3.

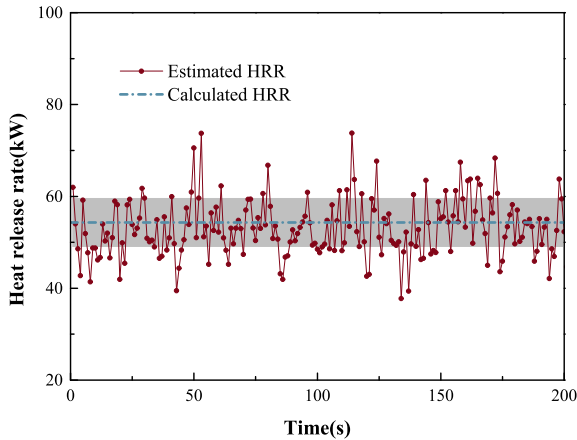


**Figure 13. Comparison diagram of estimated and calculated HRR of propane fire with time.**



### 3.5. Dynamic Analysis of Fire Development Based on Image Features

From Sect. 3.3, it can be seen that the changes of flame height, projected area, and flame volume with time are highly consistent, so the flame size characteristics involved in this paper can directly reflect the change process of HRR. However, the camera angle may lead to difficulties in obtaining accurate flame volume, which requires a precise perspective transformation in real fires. On the contrary, it is relatively simple to get flame height, but there is a deviation of height for the description of fire when the flame shape changes induced by external conditions (e.g., changes in the burned area, change in the wind speed and direction, or in a ceiling jet fire). For the projected area of flame, as long as the relatively reasonable projection plane of the camera is selected, the fire development can be reasonably characterized. Therefore, the flame projected area is adopted here to describe the fire development and directly infer the combustion stage. Take Test 3 as an example, fire curve of the wood crib is divided into four stages after flame appeared as shown in Fig. 14:

- I *Initial phase*. A fire began to form with a rapid growth rate, but the height and width of flame are small, accompanied by a lot of smoke as in the early stage of fire.
- II *Growth phase*. Since all the firewood is ignited in the I phase, fire expands rapidly with the increase in flame size and HRR gradually within this period.
- III *Steady burning phase*. The wood crib reaches a maximum HRR, and the flame height, width, area, and volume maintain within a certain range in general.
- IV *Decay phase*. The fire starts to drop quickly until wholly extinguished, with the intervention of fire water at 1210 s.

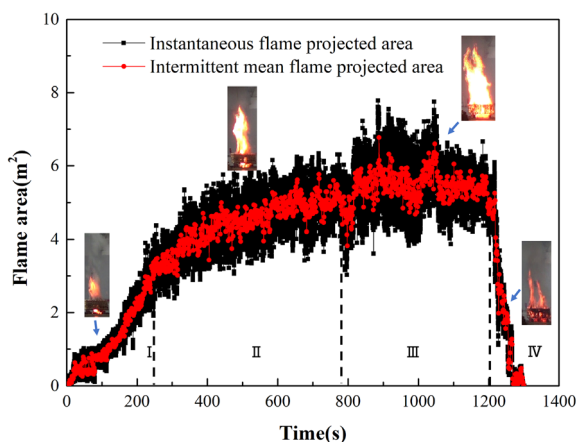


**Figure 14. Different stages of wood crib fire over time.**

## 4. Conclusions

In a sudden fire, full reconnaissance of the fire scene based on real-time information is essential for complete targeted emergency rescue. In order to provide information support from the surveillance system to emergency response and fire rescue, an intelligent information inversion model of video-driven fire has been proposed and programmed with Python in this paper, including VFD, fire characteristics extraction based on object-oriented segmentation, fire information inversion, and development analysis. By image classification, the proposed method only performs segmentation on images recognized as fire, which avoids the complex algorithm and computational cost of target detection. In addition, the speed and efficiency of segmentation are highly improved by the object-oriented method. The specific conclusions are as follows:

- (1) The SEEDS algorithm has a good effect on the segmentation of actual fire scenes. It is recommended that the setting value of superpixel should be moderate to avoid excessive computation and inaccurate segmentation caused by inappropriate value.
- (2) The model proposed in this paper can effectively achieve the real-time flame height, projected area, flame volume, and other dimensional features in actual fires.
- (3) Combined with prior fire knowledge, fire size information can be utilized to estimate the HRR and analysis fire development for different types of fires.

## Funding

Funding was provided by National Natural Science Foundation of China (Grant number 51578464).

## References

1. Ojo JA, Oladosu JA (2014) Video-based smoke detection algorithms: a chronological survey. *Compu Eng and Intell Syst* 5:38–50
2. Alkhatib AAA (2014) A review on forest fire detection techniques. *Int J Distrib Sens N*. <https://doi.org/10.1155/2014/597368>
3. Huang P-H, Su J-Y, Lu Z-M, Pan J-S (2006) A fire-alarming method based on video processing. *IIH-MSP*. <https://doi.org/10.1109/IIH-MSP.2006.265017>
4. Chen T-H, Wu P-H, Chiou Y-C (2004) An early fire-detection method based on image processing. *ICIP* 3:1707–1710. <https://doi.org/10.1109/ICIP.2004.1421401>
5. Qureshi WS, Ekpanyapong M, Dailey MN, Rinsurongkawong S, Malenichev A, Krasotkina O (2016) QuickBlaze: early fire detection using a combined video processing approach. *Fire Technol* 52:1293–1317. <https://doi.org/10.1007/s10694-015-0489-7>
6. Yang X, Wang J, He S (2012) A SVM approach for vessel fire detection based on image processing. *ICMIC* pp.150–153

7. Wang DC, Cui X, Park E, Jin C, Kim H (2013) Adaptive flame detection using randomness testing and robust features. *Fire Saf J* 55:116–125. <https://doi.org/10.1016/j.firesaf.2012.10.011>
8. Wu H, Wu D, Zhao J (2019) An intelligent fire detection approach through cameras based on computer vision methods. *Process Saf Environ Protect* 127:245–256. <https://doi.org/10.1016/j.psep.2019.05.016>
9. Zhang J, Zhu H, Wang P, Ling X (2021) Att squeeze u-net: a lightweight network for forest fire detection and recognition. *IEEE Access* 9:10858–10870. <https://doi.org/10.1109/ACCESS.2021.3050628>
10. Li P, Zhao W (2020) Image fire detection algorithms based on convolutional neural networks. *Case Stud Therm Eng* 19:100625. <https://doi.org/10.1016/j.csite.2020.100625>
11. Lin G, Zhang Y, Xu G, Zhang Q (2019) Smoke detection on video sequences using 3D convolutional neural networks. *Fire Technol* 55:1827–1847. <https://doi.org/10.1007/s10694-019-00832-w>
12. Verstockt S, Beji T, Potter PD, Sv H, Sette B, Merci B, Walle RVd (2013) Video driven fire spread forecasting (f) using multi-modal LWIR and visual flame and smoke data, *Pattern Recognit. Lett* 34:62–69. <https://doi.org/10.1016/j.patrec.2012.07.018>
13. Heskestad G (2002) Fire plumes, flame height, and air entrainment. *SFPE handbook of fire protection engineering*, 3rd ed. National Fire Protection Association, Quincy, pp 2:1–17
14. Xin Y (2014) Estimation of chemical heat release rate in rack storage fires based on flame volume. *Fire Saf J* 63:29–36. <https://doi.org/10.1016/j.firesaf.2013.11.004>
15. Li K, Mao S, Feng R (2019) Estimation of heat release rate and fuel type of circular pool fires using inverse modelling based on image recognition technique. *Fire Technol* 55:667–687. <https://doi.org/10.1007/s10694-018-0795-y>
16. Beji T, Verstockt S, Zavaleta P (2016) Merci B (2016) Flame spread monitoring and estimation of the heat release rate from a cable tray fire using video fire analysis (VFA). *Fire Technol* 52:611–621. <https://doi.org/10.1007/s10694-015-0538-2>
17. Cheng Y, Chen K, Bai H, Mou C, Zhang Y, Yang K, Gao Y, Liu Y (2021) An efficient fire detection algorithm based on multi-scale convolutional neural network. *Fire Mater.* <https://doi.org/10.1002/fam.3045>
18. Achanta R, Shaji A, Smith K, Lucchi A, Fua P, Süsstrunk S (2012) SLIC superpixels compared to state-of-the-art superpixel methods. *IEEE Trans Pattern Anal Mach Intell* 34(11):2274–2282. <https://doi.org/10.1109/TPAMI.2012.120>
19. Bergh M, Boix X, Roig G, Gool L (2015) SEEDS: superpixels extracted via energy-driven sampling. *Int J Comput Vision* 111(3):298–314. <https://doi.org/10.1007/s11263-014-0744-2>
20. Levinstein A, Stere A, Kutulakos KN, Fleet DJ, Dickinson SJ, Siddiqi K (2009) TurboPixels: fast superpixels using geometric flows. *IEEE T Pattern Anal* 31(12):2290–2297. <https://doi.org/10.1109/TPAMI.2009.96>
21. Chen J, Li Z, Huang B (2017) Linear Spectral Clustering Superpixel. *IEEE Trans Image Process* 26:3317–3330. <https://doi.org/10.1109/TIP.2017.2651389>
22. Ban Z, Liu J, Fouriaux J (2018) GLSC: LSC superpixels at over 130 FPS. *J Real-time Image Pr* 14(3):605–616. <https://doi.org/10.1007/s11554-016-0652-5>
23. Celik T, Demirel H (2009) Fire detection in video sequences using a generic color model. *Fire Saf J* 44(2):147–158. <https://doi.org/10.1016/j.firesaf.2008.05.005>
24. Orloff L (1981) Simplified radiation modeling of pool fires. *Proc Combust Inst* 18(1):549–561. [https://doi.org/10.1016/S0082-0784\(81\)80060-4](https://doi.org/10.1016/S0082-0784(81)80060-4)
25. Orloff L, De Ris J (1982) Froude modeling of pool fires. *Proc Combust Inst* 19(1):885–895. [https://doi.org/10.1016/S0082-0784\(82\)80264-6](https://doi.org/10.1016/S0082-0784(82)80264-6)

26. Hu L, Huo R, Wang H, Li Y, Yang R (2007) Experimental studies on fire-induced buoyant smoke temperature distribution along tunnel ceiling. *Build Environ* 42(11):3905–3915. <https://doi.org/10.1016/j.buildenv.2006.10.052>
27. Linteris GT, Rafferty I (2008) Flame size, heat release, and smoke points in materials flammability. *Fire Saf J* 43:442–450. <https://doi.org/10.1016/j.firesaf.2007.11.006>
28. Zhang X, Hu L, Wang Q, Zhang X, Gao P (2015) A mathematical model for flame volume estimation based on flame height of turbulent gaseous fuel jet. *Energy Convers Manag* 103:276–283. <https://doi.org/10.1016/j.enconman.2015.06.061>
29. Wang J, Fang J, Guan J, Zeng Y, Zhang Y (2016) Flame volume and radiant fraction of jet diffusion methane flame at sub-atmospheric pressures. *Fuel* 167:82–88. <https://doi.org/10.1016/j.fuel.2015.11.049>
30. Liu M, Tuzel O, Ramalingam S, Chellappa R (2011) Entropy rate superpixel segmentation. *Proc IEEE Comput Vis Pattern Recognit*. <https://doi.org/10.1109/CVPR.2011.5995323>
31. Kostiuk LW, Mejeski AJ, Poudenx P, Johnson MR, Wilson DJ (2000) Scaling of wake-stabilized jet diffusion flames in a transverse air stream. *Proc Combust Inst* 28(1):553–559. [https://doi.org/10.1016/S0082-0784\(00\)80255-6](https://doi.org/10.1016/S0082-0784(00)80255-6)
32. De Ris J, Wu P, Heskestad G (2000) Radiation fire modeling. *Proc Combust Inst* 28(2):2751–2759. [https://doi.org/10.1016/S0082-0784\(00\)80696-7](https://doi.org/10.1016/S0082-0784(00)80696-7)
33. Stratton BJ (2005) Determining flame height and flame pulsation frequency and estimating heat release rate from 3D flame reconstruction. Dissertation, University of Canterbury. <https://doi.org/10.1111/j.1471-0307.1951.tb02096.x>